Optogenetic Assessment of VIP, PV, SOM, and NOS Inhibitory Neuron Activity and Cerebral Blood Flow Regulation in Mouse Somato-sensory Cortex

by

Michael B. Krawchuk

Neuroscience, University of Pittsburgh, 2019

Submitted to the Graduate Faculty of

The University Honors College

of the requirements for the degree of

Bachelor of Philosophy

University of Pittsburgh

2019

UNIVERSITY OF PITTSBURGH

DIETRICH SCHOOL OF ARTS AND SCIENCES

This thesis/dissertation was presented

by

Michael B. Krawchuk

It was defended on

April 1, 2019

and approved by

Dr. Caroline Runyan, Assistant Professor, Neuroscience

Dr. Mitsuhiro (Hiro) Fukuda, Assistant Professor, Radiology

Dr. Edith Hamel, Professor, Neurology and Neurosurgery

Thesis Advisor/Dissertation Director: Dr. Alberto Vazquez, Associate Professor, Radiology and Bioengineering

Optogenetic Assessment of VIP, PV, SOM, and NOS Inhibitory Neuron Activity and Cerebral Blood Flow Regulation in Mouse Somato-sensory Cortex

Michael B. Krawchuk, Bphil

University of Pittsburgh, 2019

The impact of different neuronal populations on local cerebral blood flow (CBF) regulation is not well known and insight into these relationships could enhance the interpretation of brain function and dysfunction from brain imaging data. We investigated the role of sub-types of inhibitory neurons on the regulation of CBF using optogenetics, laser Doppler flowmetry and different transgenic mouse models (parvalbumin (PV), vasoactive intestinal peptide (VIP), somatostatin (SOM) and nitric oxide synthase (NOS)). Whisker stimulation was used to verify that typical CBF responses were obtained in all mice (average increase of 14%). Photo-stimulation of SOM-cre and NOS-cre mice produced significant increases in CBF that were similar to whisker responses. In NOS-cre mice, CBF responses scaled with the photo-stimulus pulse duration and frequency. In SOM-cre mice, CBF increases were followed by decreases. In VIP-cre mice, photo-stimulation did not consistently produce significant changes in CBF, while slower increases in CBF that peaked 14-18 seconds after stimulation onset were observed in PV-cre mice. Control experiments performed in non-expressing regions showed no changes in CBF. These findings suggest that dysfunction in NOS or SOM expressing neurons can have a significant impact on CBF responses that could be detected by brain imaging methods like fMRI.

Table of Contents

List of Tables

List of Figures

Preface

I would like to acknowledge my collaborating authors: Dr. Xiaoling Yang (Department of Radiology), Dr. Catherine A. Ruff (Department of Neurobiology), Dr. Sarah E. Ross (Department of Neurobiology). This work was supported by NIH grants R01-NS-094404 (to AV), F31-NS106764 (to CR) and R01-AR063772 (to SR). We would like to thank the Center for Biological Imaging (CBI) of the University of Pittsburgh for their help imaging histological samples. Also, we would like thank Dr. Deisseroth and the University of North Carolina Viral Vector Core for generously providing and facilitating access to the optogenetic constructs used in this work. My collaborators, advisor and I have no conflicts of interest to declare.

1.0 Introduction

The mammalian brain consists of numerous neuronal and non-neuronal cell types whose function is supported by an extensive network of blood vessels. Neurons are the main processing unit in the brain, coordinating and processing complex functions, including movement, memory and cognition. Neurons do not store substrates for energy generation and require a continuous supply of blood to provide them with oxygen and glucose for energy. It has been shown that different levels of activity elicit commensurate changes in cerebral blood flow [1-3]. In fact, human brain imaging studies, such as BOLD fMRI (Blood Oxygen Level Dependent Functional Magnetic Resonance Imaging), use these changes in blood flow and blood oxygenation to infer neural activity. There is increasing evidence that certain types of neurons can play a significant role in blood flow regulation [4-9]. For example, slice experiments show vaso-dilatory and -constrictive effects from stimulation of vasoactive intestinal peptide (VIP) and somatostatin (SOM) expressing interneurons, respectively [5]. Understanding what types of neurons regulate cerebral blood flow will provide vital insight for a more accurate interpretation of fMRI data in health and disease conditions. Since brain disorders are often associated with neuronal dysfunction which can alter functional hyperemic changes [10-13], understanding the role of different neuronal sub-types on cerebral blood flow might enable the use of CBF or BOLD fMRI data to detect brain dysfunction as well as monitor disease progression.

There are two general types of neurons, excitatory and inhibitory. Excitatory neurons propagate activity to their connected network, which includes inhibitory neurons. Inhibitory neurons suppress the propagation of spiking activity via the release of the neurotransmitter GABA (gamma amino-butyric acid). They work to shape and restrict the activity encoded by neural

networks. In addition, it is known that some inhibitory neurons can release vasoactive molecules, such as nitric oxide (NO), which is generated by the activity of the enzyme nitric oxide synthase (NOS). It has also been reported that some inhibitory neurons are located close to intra-cortical arterial vasculature [5, 14]. These properties position inhibitory neurons as potentially vital regulators of local blood supply. Numerous signaling pathways have been identified, both direct and indirect, by which neuronal activity can produce local changes in arterial diameter and blood flow [6] . Since the arterio-venous pressure difference is roughly constant, blood flow regulation is essentially accomplished via dilation and constriction of vascular contractile elements (e.g. smooth muscle) in cerebral arteries, arterioles and some capillary segments [15-18]. Studies focusing on excitatory neurons (glutamatergic) have shown they release vasoactive molecules, such as prostaglandin E2, following pyramidal cell and NMDA receptor activation [19, 20]. Studies focusing on inhibitory neurons have shown they can increase local cerebral blood flow separately from excitatory neuron activity [5, 8, 9, 14]. It is evident from these studies that all neurons do not regulate blood flow in the same manner, and that not all neurons may be capable of generating changes in local perfusion.

The goal of this work is to determine the role of some populations of inhibitory neurons on cerebral blood flow (CBF) regulation. To this end, we used cre-recombinase transgenic mouse lines that target different populations of inhibitory neurons to insert the optogenetic protein Channelrhodopsin-2 (ChR2) by viral transduction to directly stimulate the cells of interest using narrow-band light (e.g. 473 nm). We performed the experiments in mice that express ChR2 in the following protein targets of inhibitory neurons: Parvalbumin (PV), Vasoactive Intestinal Peptide (VIP), Somatostatin (SOM or SST) and Nitric Oxide Synthase (NOS). These genetic targets are not all independent, mice targeting PV- and VIP-expressing neurons show little overlap [21, 22],

while NOS neurons are a subset of SOM neurons (particularly type I) [23, 24]. Whisker stimulation was used for comparison in these studies. The following guiding hypotheses were considered: (1) inhibitory neuron populations expressing NOS are able to regulate CBF in a dose-dependent manner, (2) inhibitory neuron populations that do not express NOS do not have a significant impact on CBF regulation, and (3) inhibitory neuron populations capable of firing at high rates (i.e. PV) can regulate CBF in a dose-dependent manner but only at high stimulation frequencies (likely due to metabolic depletion).

2.0 Materials and Methods

2.1 Animal Preparation

A total of 23 mice (male, 23-32 g; 3-9 months old) were obtained from the Jackson Laboratory (Bar Harbor, ME) coding for the enzyme cre-recombinase in the genome of the targeted inhibitory neurons (PV, n=6 strain B6.129P2-Pv(albtm1(cre)Arbr)/J; VIP, n=7 strain VIP(tm1(cre)Zjh)/J; SST, n=5 strain B6N.Cg-SST(tm2.1(cre)Zjh]/J; NOS, n=5 strain B6.129S-Nos1(tm1.1(cre/ERT2)Zjh)/J). All procedures performed followed an experimental protocol approved by the University of Pittsburgh Institutional Animal Care and Use Committee (IACUC) in accordance with the standards for humane animal care and use as set by the Animal Welfare Act (AWA), the National Institute of Health Guide for the Care and Use of Laboratory Animals and ARRIVE (Animal Research: Reporting in Vivo Experiments). Expression of the optogenetic protein Channelrhodopsin-2 (ChR2) was achieved by intra-cortical injection with AAV-DIO-ChR2(H134R)-YFP obtained from the University of North Carolina Viral Vector Core. Mice were anesthetized with ketamine (75 mg/kg) and xylazine (10 mg/kg) and placed in a stereotaxic frame (Narishige Inc., Tokyo, Japan) for craniotomy, head-plate installation, and viral injection. Supplementary oxygen (40% balanced by air) was administered via nose cone at 500 mL/min. Body temperature was maintained at 38°C (measured under the abdomen) using a DC feedback unit. Surgery consisted of removing the skin over the skull and exposing the bone until dry. The aluminum head plate (Narishige Inc.) contains an 8 mm round opening that was positioned over the area of interest and then the plate was cemented onto the skull using VetBond (3M Inc.) and dental cement. A craniotomy 4-mm in diameter was performed over the somatosensory cortex

centered around 3 mm lateral and 1.5 mm posterior from the Bregma. Mice were then placed under the microscope to visualize the virus injection (Figure 1A and 1B). A glass micro-pipette was used to inject small amounts of virus at depths of 300µm and 600µm into the somato-sensory cortex. A small amount of fluorescent dye (200µM SR-101) was used to visualize virus delivery in the targeted locations. The total injected volume was about 0.1µl. A custom cover glass consisting of a 4-mm round cover glass glued on a 5-mm round cover glass (CS-4R and CS-5R, Warner Instruments Inc.) was cemented onto the skull to maintain visual access to the brain. Aseptic procedures were followed and mice were allowed 2 weeks for recovery. During recovery the mice were acclimated to a custom treadmill for awake head-fixed data collection. The NOS mouse model is an inducible cre-line and tamoxifen was administered one-week post-surgery following protocol described in the Jackson Laboratory's website.

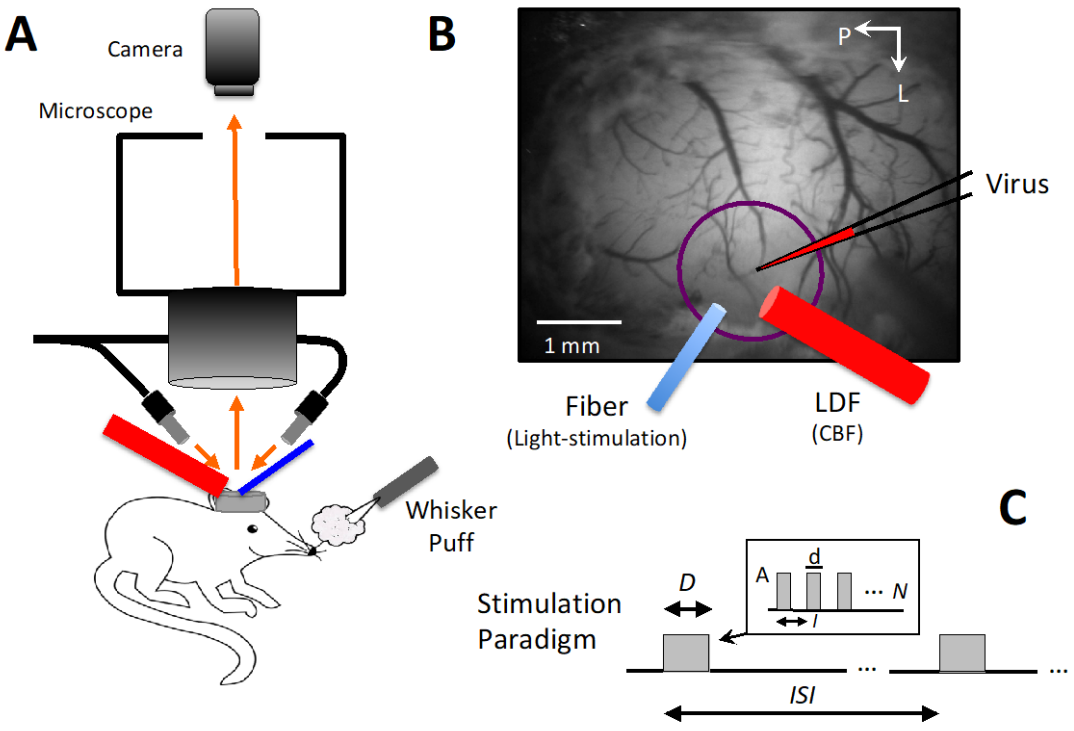

Figure 1 - Experimental setup and experimental paradigm description.

2.2 Probe Placement

A fluorescence microscope (MVX-10, Olympus Inc., Japan) was used to identify the ChR2-YFP expression region (whisker somato-sensory cortex). A Laser Doppler Flowmeter (LDF; Periflux 5000/411, Perimed AB, Jarfalla, Sweden) and an optic fiber (S-405-HP, core diameter of 125μm; ThorLabs, Inc., Newton, NJ) were placed over the cover glass facing the expressing region while avoiding large surface vessels (Figure 1A and 1B). LDF was used to acquire cerebral blood flow (CBF) data and the optic fiber was used to deliver the photo-stimulus. The LDF probe used has a tip diameter of 450μm and operating wavelength of 780nm. Because each probe was placed under the fluorescence microscope, the fiber and probe were placed at a 60° angle. An air puffer was also placed in front of the contralateral whisker pad to stimulate the somato-sensory cortex (Figure 1A).

2.3 Experimental Design

Photo-stimulation and whisker stimulation experiments were performed in all animals under awake head-fixed conditions. The photo-stimulus was delivered using a power-adjustable, TTL-controlled, 473nm laser diode unit (CrystaLaser Inc., Reno, NV) connected to the optic fiber. The laser power at the tip of the fiber was set to 1 mW measured using a power meter (Melles Griot 13PM001, IDEX Inc., Rochester, NY). Air puffs were delivered using a pressure injector (Toohey Spritzer, Toohey Company, Fairfield, NJ) set to 30 psi. The photo-stimulus pulse

duration and frequency were varied to modulate the amount of evoked activity and examine its impact on hemodynamic responses. The photo- or whisker stimulation paradigm is described in Figure 1C. In short, pulses of light (d=30, 10 or 2 ms in duration; A=1mW) were delivered at an interval (I) corresponding to frequencies of either 5, 10, 20 or 40 Hz over a stimulation period (D) of either 1 second every 30 seconds (inter-stimulus interval or ISI) or 4 seconds every 40 seconds. At least 10 stimulation trials were collected for each stimulation parameter set. These photo-stimulation parameters were selected based on previous experiments from our group [9, 25] . For whisker stimulation, the pulse duration and frequency were fixed to 50 ms and 5 Hz, respectively. Although photo-stimulation and whisker stimulation initiate cortical activity in different neuronal populations (inhibitory and excitatory, respectively), whisker stimulation allowed us to establish that the physiological neurovascular mechanism was not disrupted. Additional experiments were conducted in a subset of mice to serve as control experiments. In these experiments, the optic fiber and LDF probe were positioned in a non-expressing region of the visible cortex. Stimulation triggers and LDF data were recorded at 1 kHz (MP150, Biopac Systems Inc., Goleta, CA).

2.4 Data Analysis

All data were analyzed using Matlab (Mathworks, Natick, MA, USA). Time series of the changes in cerebral blood flow evoked by whisker or photo-stimulation were obtained from the LDF data. Time series spanning 40 seconds were obtained from all trials starting 5 seconds prior to stimulation onset. The LDF time series were low-pass filtered with a rectangular cut-off of 4 Hz and down-sampled to 10 Hz. Small linear trends were removed from each trial by considering only data over the 4 seconds preceding stimulation onset (baseline) and the last 4 seconds of each

trial. Lastly, time series from trials with common stimulation parameters were averaged and then normalized by their pre-stimulation baseline level. Changes in CBF were measured from the average time series as the average value 1 to 4 seconds after stimulation onset (for 1-sec photo-stimulation) or 4 to 7 seconds after photo-stimulation (for 4-sec photo-stimulation). The time-to-peak was also measured directly from the time series. Significant differences in CBF response amplitude were tested relative to baseline using a t-test ($p<0.05$). In addition, linear regression analyses were performed on the CBF amplitude as a function of pulse duration and frequency to test for significant relationships using a mixed effects model ($p<0.05$). We considered a particular inhibitory neuron population to play a significant role in regulating CBF if photo-stimulation evoked significant changes from baseline in 4 out of 6 parameters tested and showed a significant relationship to either pulse duration or frequency. We report average values ± standard deviation when available, while the error bars in the figures denote the standard error.

2.5 Immunostaining

Mice were anesthetized with sodium pentobarbital (Euthasol Solution, Virbac Animal Health Inc., Fort Worth, TX) and sacrificed by transcardial perfusion with 0.1 M phosphate buffer solution (PBS) followed by perfusion with 4% paraformaldehyde (PFA; EMS, Hatfield, PA, USA) in 0.1 M PBS (pH 7.4). Brains were removed and fixed in 4% PFA solution overnight at 4°C, and then left in 30% sucrose for two nights at 4°C. Sections were cut on a freezing microtome from frontal to parietal cortex covering the cranial window area and series of 20 to 50 μm thick coronal sections were mounted on Superfrost Plus slides for storage at -80°C until use, or collected into a 24 well culture plate filled with PBS for storage at 4C. Glass or free-floating sections were washed

three times in PBS for 5 min each and were blocked and permeabilized overnight at 4 °C in a solution containing 0.2% Triton X-100, 5% bovine serum albumin and 10% donkey serum in PBS. The following primary antibodies were then applied for 72 hrs at 4°C: YFP (1:500, chicken anti-GFP polyclonal, ab13970, Abcam Inc., Cambridge, MA), Parvalbumin (1:500 rabbit anti-parvalbumin polyclonal, ab11427 Abcam), VIP (1:600, rabbit anti-VIP polyclonal, Immunostar, Hudson, WI), SOM (1:600, rabbit anti-SST polyclonal, HPA019472 Sigma-Aldrich, St. Loius, MO), NOS (1:500, goat anti-NOS1 polyclonal, NB100-858, Novus Biologicals, LLC, Centennial, CO). After washing in PBS for 30 min, the tissue was incubated with the cross-absorbed secondary antibody donkey anti-chicken Alexa488 for YFP, donkey anti-goat Alexa594 for NOS, and donkey anti-rabbit Alexa594 for PV, SOM, and VIP for 2 hours at room temperature with secondary antibodies diluted 1:500 in PBS. The slides were thoroughly rinsed in PBS before sections were mounted with cover glass.

Immunostained sections were imaged by confocal microscopy (Nikon A1 Spectral Confocal, Japan) using a 40× objective lens. Imaging settings were optimized to eliminate background staining in all channels after calibrating the laser intensity, signal offset and amplifier gain on slices treated without primary antibody. Other than making moderate adjustments for contrast and brightness, the images were not manipulated. Images were acquired from sections covering the YFP expressing region in the somato-sensory cortex (4-5 sections). We used ImageJ (NIH, USA) to analyze the images and count cell expression.

3.0 Results

All animals injected with AAV-DIO-ChR2(H134R)-YFP showed expression of Channelrhodopsin-2 in somato-sensory cortex around one week post-injection. Expression was verified using fluorescence microscopy (Figures 2A-D) and two-photon microscopy as evidenced by the fluorescence of YFP along cell membranes (Figures 2E-H). Experiments were performed after the expression stabilized, 2-3 weeks post-injection, during which time they were acclimated to our awake head-fix treadmill for experimentation.

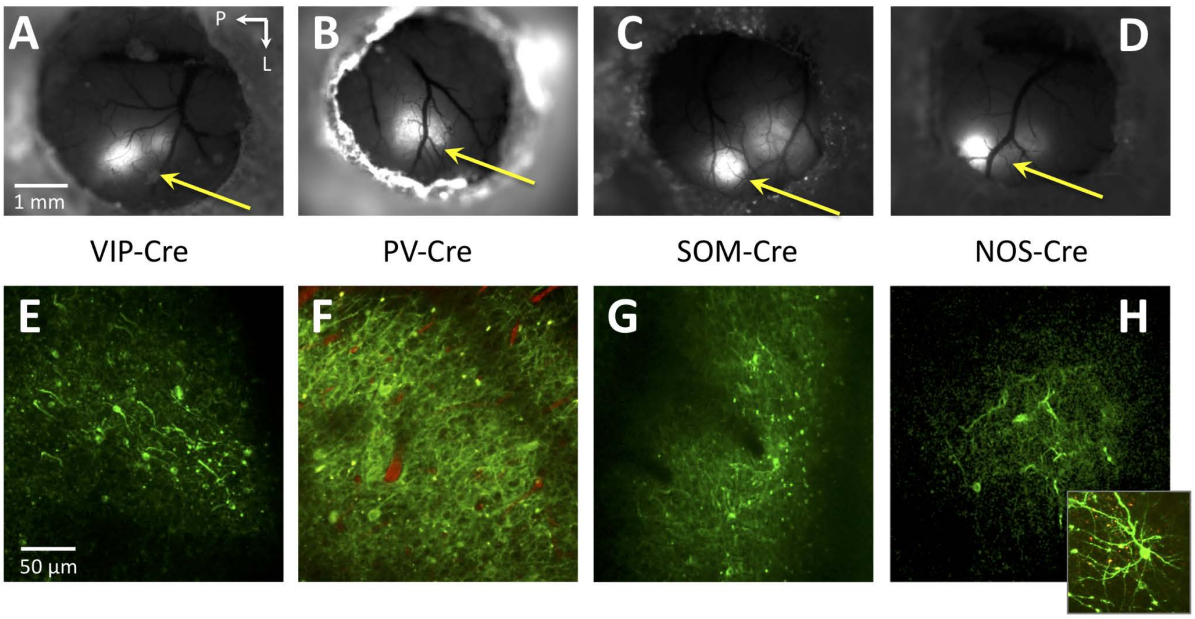

Figure 2 - Fluorescence microscopy images over the entire cranial window (A-D) as well as high resolution two-photon microscopy maximum intensity projection images (E-H).

3.1 Expression Assessment

To determine the specificity of the neuronal populations targeted, we first describe the expression profile by immunostaining. In VIP-cre mice, expression was similar to previous reports [26, 27]. Bitufted anatomical features were evident in VIP and YFP labeled cells (Figure 3A). There was a tendency for VIP cells to preferentially exist in Layers II/III, although immunostaining also showed them in high numbers in deeper layers. Counter-staining for YFP showed that most of ChR2-YFP(+) cells in this region were also VIP+ (71.5%, Table 1). In general, VIP immunostaining was faint and positive identification often required verification among adjacent sections. Many of the YFP+/VIP- cells appeared to have bitufted anatomical features suggesting that these cells are also VIP+ but the staining was sufficiently faint to prevent positive identification. Nonetheless, a large fraction of YFP+ cells were also VIP+.

In PV-cre mice, expression was similar to that published in this mouse model [21, 22, 28]. PV+ cells were found in higher numbers in middle and deeper cortical layers (Figure 3B). Counter-staining for YFP expression showed co-labeled PV+ cells in this region, especially in deeper layers (Figure 3B). Quantification of labeled cells showed that 86% of YFP+ cells were also PV+ (Table 1). No apparent preference for YFP+/PV- negative was observed, also these cells did not appear to be pyramidal based on negative long-range projections extending out of this region.

In SOM-cre mice, SOM and YFP immunostaining showed large numbers of positive cells throughout the somato-sensory cortex. Labeled cells spanned layers II-VI, with higher preference to Layer II/III (Figure 3C). Co-labeling for YFP showed that most YFP+ were also SOM+ (69.2%, Table 1 and Figure 3C). Our findings are in agreement with previous reports for the distribution

of somatostatin neurons [21, 23, 24]. However, of the different mouse lines studied, this one showed the largest fraction of YFP+/SOM- cells. This is partly due to faint SOM staining.

In NOS-cre mice, NOS+ cells were also found throughout the cortex, similar to SOM expressing cells (Figure 3D). YFP co-labeling showed some cells with significant arborization that remained in the local region and most cells were present in upper Layer II/III and also Layer VI (Figure 3D). This is consistent with previous reports indicating that NOS+ cells can be preferentially located in these layers [23, 29]. Most YFP+ neurons were also NOS+ (73.8%, Table 1) and, similar to the other models, no evident features from other cells types for YFP+/NOS- cells were observed. We also observed high and low expressing NOS neurons in some sections, in agreement with previous reports of Type I and II NOS populations.

Table 1 - Immunostaining summary of the number of neurons expressing ChR2-YFP (YFP-positive or YFP+) in the different inhibitory neuron types of interest (INTI).

Inhibitory Neuron Type of Interest (INTI)	YFP+ (#)	YFP+/INTI+ (#) (overlap)	YFP+/INTI- (#) (no overlap)	% YFP+/INTI+
VIP (n=1)	277	198	79	71.5%
PV (n=3)	661	569	92	86.1%
SOM (n=2)	273	189	84	69.2%
NOS (n=1)	222	164	58	73.8%

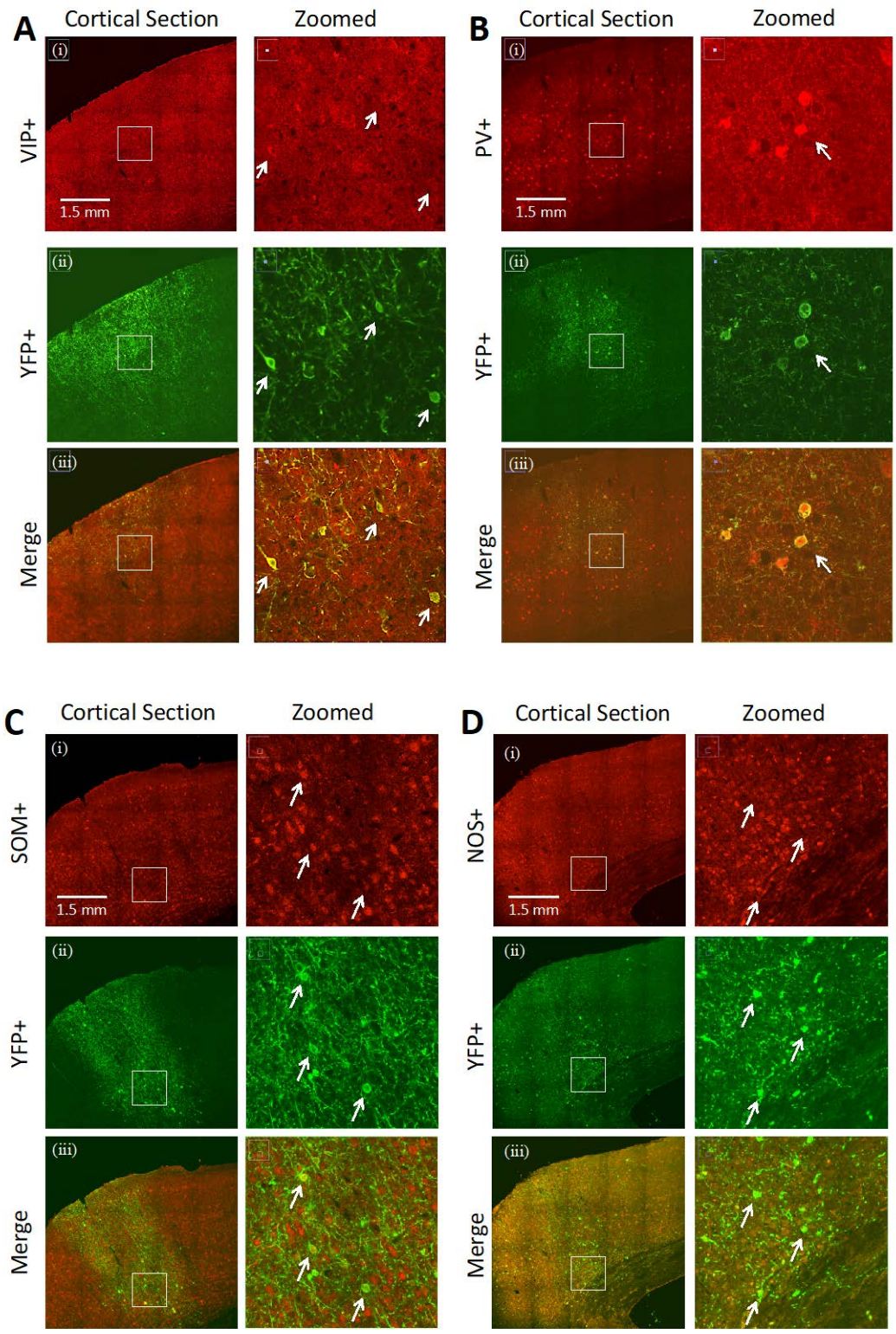

Figure 3 - Confocal images of immunostained brain sections from (A) PV-cre, (B) VIP-cre, (C) SOM-cre and (D) NOS-cre mice.

3.2 Whisker and Photo-stimulation of VIP-, PV-, SOM- and NOS-cre mice

Whisker stimulation for 1 or 4 seconds evoked detectable CBF responses in all mice. On average, 1-second whisker stimulation generated increases in CBF of 9.8% ± 9.2%, 22.7% ± 14.2, 11.0% ± 7.5% and 19.2% ± 12.8% in PV-cre, VIP-cre, SOM-cre and NOS-cre mice, respectively, while 4-second whisker stimulation generated increases in CBF of 6.8% ± 9.6%, 16.7% ± 9.4%, 12.3% ± 11.0% and 10.0% ± 10.0% in these mice, respectively. The time-to-peak measured from the average LDF responses were 3.0±2.0, 2.4±1.1, 2.7±1.7 and 2.4±1.2 seconds to 1-second stimulation and 2.7±1.6, 3.0±1.2, 3.5±2.1 and 2.4±0.9 seconds to 4-second stimulation from the different transgenic models, respectively. Collectively, whisker stimulation induced significant CBF responses with typical temporal features in all mice indicating that the neurovascular mechanism has not been perturbed.

In VIP-cre mice, photo-stimulation for 1-sec appeared to evoke small increases in CBF detectable after the stimulation period (Figure 4A). These responses peaked around 2-seconds after stimulation onset when present, and peaked faster than the whisker response. Fast changes in LDF signal around photo-stimulation (shaded blue bar in Figure 4) onset and off-set are artifactual and due to interference between the LDF probe and the photo-stimulus. However, only the CBF response evoked by 10 ms photo-stimuli showed a significant increase (Figure 5A). The amplitude of the CBF changes appeared to scale with the photo-stimulus pulse duration for 1-sec photo-stimulation (Figure 5E), but this trend was not significant ($p>0.05$) and not present for responses evoked by 4-sec photo-stimulation (Figure 5G). On the other hand, the amplitude of the CBF response scaled with the photo-stimulus frequency for 1-sec photo-stimulation ($p<0.05$; Figure 5B) but not 4-sec photo-stimulation (Figures 5F, 5H and Supplementary Figure 1).

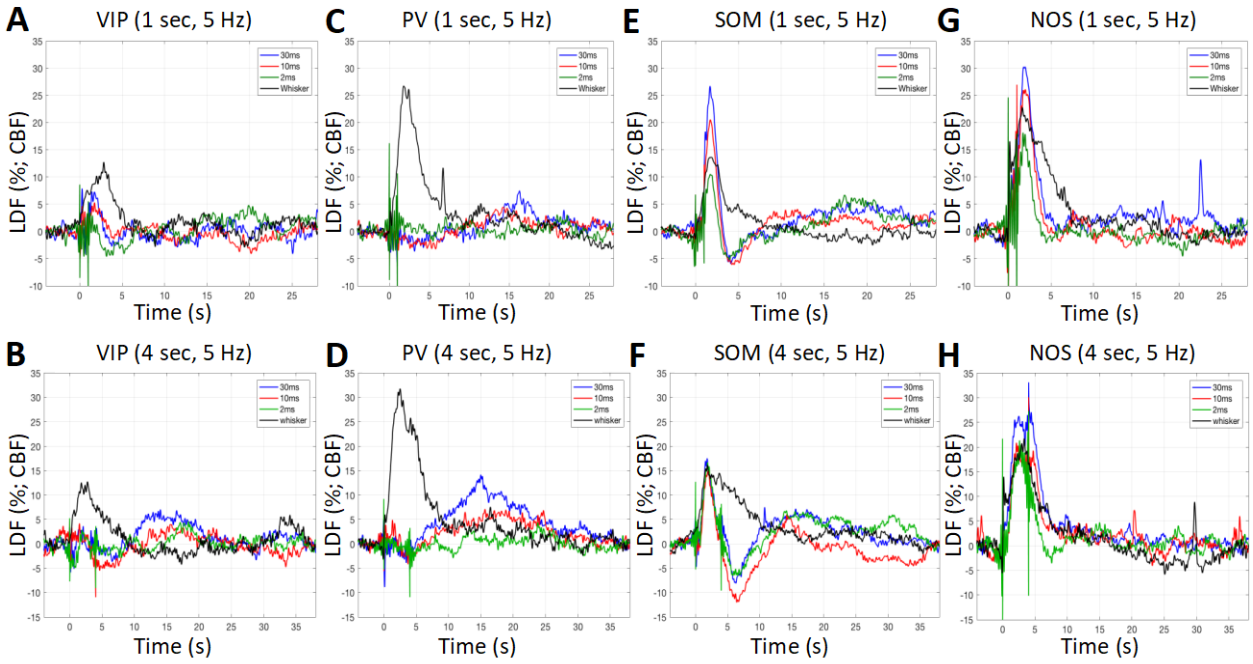

Figure 4 - Average CBF responses to photo and whisker stimulation of varying pulse widths for 1 sec (A,C,E,G) and 4 sec (B,D,F,H) pulse durations.

In PV-cre mice, photo-stimulation for either 1 or 4 seconds at 5 Hz did not evoke typical CBF responses (Figure 4C, 4D), especially when compared to the responses evoked by whisker stimulation (Figure 5A, 5C). Evident latent increases in CBF were observed 14 to 18 seconds after stimulation onset where the amplitude depended on the stimulus and pulse durations, where 4-second photo-stimulation with 10ms and 30ms pulses produced evident latent increases in CBF (Figure 4D vs. 4C). Similar atypical responses were obtained with photo-stimulation at higher frequencies where increases were observed following stimulation. This slower and latent CBF increase was observed especially with higher stimulation frequency (20 and 40Hz; Supplementary Figure 1D vs. 1C). Linear regression analyses showed no relationship between the CBF response amplitude immediately after stimulation and the photo-stimulus pulse duration or frequency ($p>0.10$) except for 4-second photo-stimulation at different frequencies ($p<0.05$; Figures 5E, 5H).

However, the relationship between the latent CBF response (14 to 18 seconds after stimulation onset) and the stimulation frequency were significant ($p<0.05$) for 1- and 4-second photo-stimulation experiments.

Different to VIP-cre and PV-cre mice, 1 and 4 second photo-stimulation at 5Hz in SOM-cre mice evoked evident increases in CBF (Figures 4E, 4F). Temporally, the increase in CBF that follows stimulation onset peaked between 1.7 and 2.1 seconds for both 1 and 4- second photo-stimulation periods. In addition, the increase in CBF was consistently followed by decreases in CBF below pre-stimulation baseline levels that bottomed around 4 seconds for 1-sec photo-stimulation and around 6 seconds for 4-second photo-stimulation. For the 1-sec photo-stimulation experiments, the CBF response amplitude was significantly modulated by the photo-stimulus pulse width ($p<0.05$, Figure 5E) and frequency ($p<0.05$, Figure 5F). No significant relationships were observed for the CBF response amplitude following 4-second photo-stimulation or for the magnitude of the observed post-stimulation decrease in CBF. The CBF increase evoked by 4-second stimulation occurred during the photo-stimulation period (shaded blue region), which is artifactually impacted by the photo-stimulus but mostly restricted to the onset and offset periods (Figure 4F and Supplementary Figure 1F). For this reason, we only considered CBF responses following the stimulation period (Figure 5G). More importantly, a latent increase similar to that observed in PV-cre mice was also observed around 15 seconds following stimulation onset that was significantly ($p<0.05$) modulated by the stimulation frequency (Supplementary Figure 1F).

For NOS-cre mice, photo-stimulation for 1 and 4 seconds also generated significant increases in CBF that shared similarities with the responses obtained in SOM-cre mice, but with notable differences. NOS-cre mice showed robust increases in CBF following optogenetic stimulation, but did not show a decrease or latent increase following photo-stimulation (Figures

4G, 4H and Supplementary Figure 1G, 1H). Increasing the frequency of 4-second photo-stimulation did induce prolonged CBF increases that returned to baseline 25 to 30 seconds after stimulation onset (vs. 5 to 10 seconds for all other responses in NOS mice). The peak CBF response was between 1.8 and 2.3 seconds for 1-sec photo-stimulation and between 2.7 and 4.8 seconds for 4-sec photo-stimulation. Linear regression analyses showed significant relationships between CBF response and all photo-stimulation parameters tested (Figure 5). Interestingly, photo-stimulation for 1 or 4 seconds with pulse durations of 10 or 30 ms produced CBF responses that were similar (or larger) in magnitude to whisker-evoked CBF responses. Similar increases were also observed in SOM-cre mice. Photo-stimulation of NOS-cre mice for longer pulse durations or stimulation frequencies produced the largest CBF increases out of all the mouse models tested (Figure 5B and D).

Lastly, data acquired from non-expressing regions in these mice did not show significant changes in CBF following photo-stimulation to any of the parameters tested (Supplementary Figure 2). These findings are in agreement with previous studies by our group using similar photo-stimulation parameters [25].

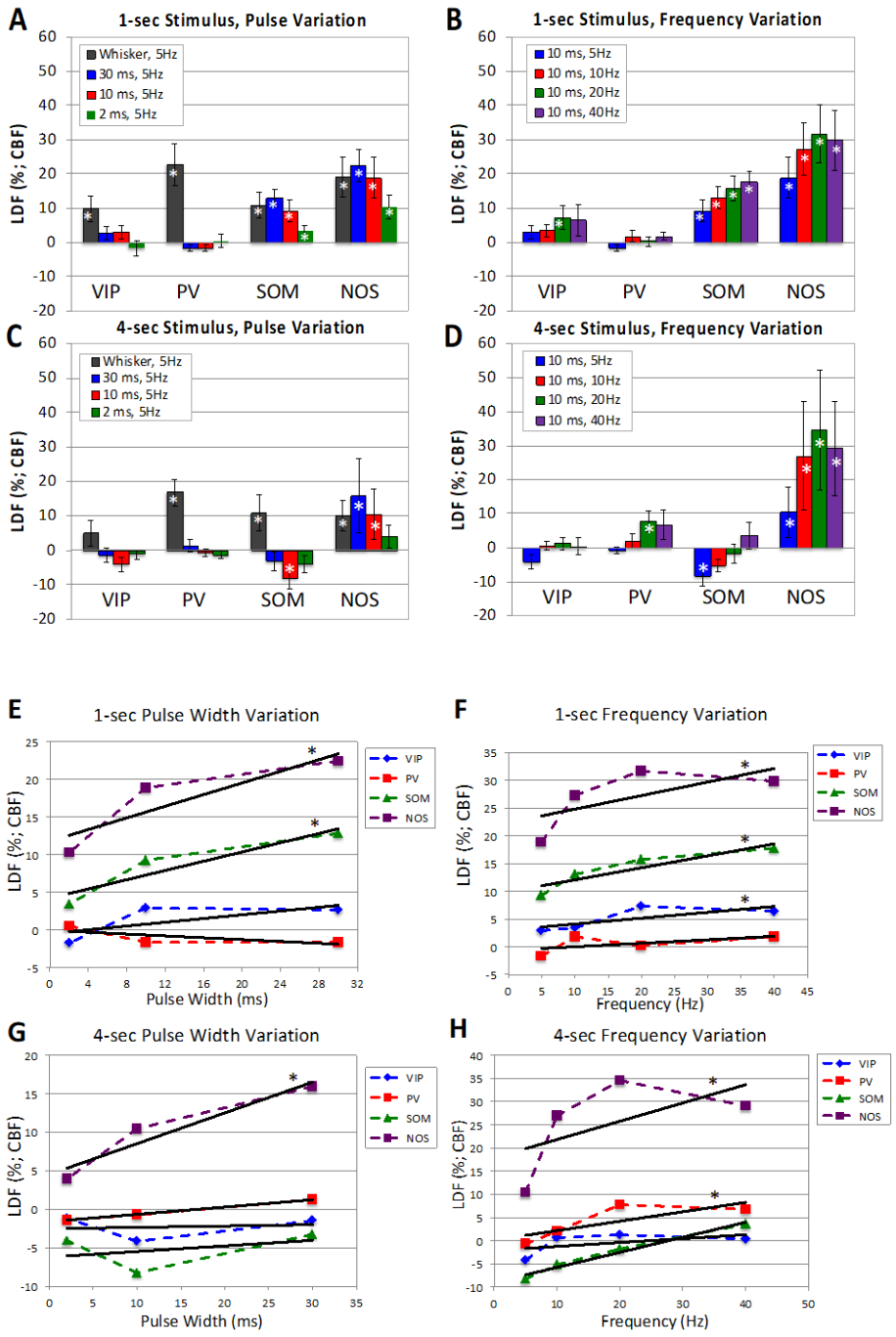

Figure 5 - Summary of the changes in CBF evoked by photo-stimulation in the different transgenic mouse models used (A-D) and linear regression analysis comparing CBF response to increasing pulse width (E and G) or frequency (F and H).

4.0 Discussion

We investigated the role of sub-types of inhibitory neurons on the regulation of cerebral blood flow using different transgenic mouse models (PV-cre, VIP-cre, SOM-cre and NOS-cre). Channelrhosopin-2 expression was virally expressed in somato-sensory cortex. To ensure the neurovascular mechanisms were not perturbed by surgery or viral transduction, whisker stimulation was used to verify that typical CBF responses were obtained in all transgenic mice. We observed typical CBF responses evoked by whisker stimulation, with average peak amplitude of 14% taking place 2 to 4 seconds following onset and subsided 10 to 15 seconds after stimulus cessation. Photo-stimulation of SOM-cre and NOS-cre mice produced significant increases in CBF that were similar to that evoked by whisker stimulation. Photo-stimulation in NOS-cre mice produced significant CBF responses (overall average increase of 21.8%) that scaled with the stimulus pulse duration and frequency. The amplitude of the CBF responses in these mice were similar to those produced by whisker stimulation; however, in SOM-cre mice CBF increases (12.0% on average) were followed by significant decreases below pre-stimulation baseline. Photo-stimulation in VIP-cre mice did not produce significant changes in CBF except for 1-second photo-stimulation at frequencies over 5 Hz. Also, photo-stimulation in PV-cre mice did not produce typical increases in CBF, rather slow and latent increases in CBF were observed that scaled with stimulus duration and frequency and peaked 14 to 18 seconds after stimulation onset. Control experiments performed in non-expressing regions of these mice showed no changes in CBF following photo-stimulation. Collectively, our results indicate that NOS expressing inhibitory neurons are able to strongly regulate local CBF, while SOM expressing inhibitory neurons can both increase and decrease CBF. On the other hand, VIP and PV expressing neurons do not appear

to play a significant role in local CBF regulation. These findings build on previous studies to clarify the role and impact of sub-populations of neurons on local blood flow regulation. More importantly, our findings suggest that dysfunction in NOS or SOM expressing neurons can have a significant impact on CBF responses that could be detected by CBF-sensitive brain imaging methods, like BOLD, CBF or CBV fMRI (e.g. arterial spin labeling fMRI or ASL fMRI).

Two-photon microscopy images acquired prior to experimentation revealed numerous ChR2-YFP neurons in the somato-sensory cortex of all models used. Immunostaining post-experimentation verified that the mouse models successfully targeted large fractions of the inhibitory neuron cell types of interest (INTI). We cannot rule out the possibility that non-overlapping YFP+ expression can introduce unwanted, non-specific responses. We believe non-specific effects are not significant for several reasons. First, anatomical assessment of this population cells (YFP+/INTI-) did not reveal long-range connections to thalamus or the contra-lateral hemisphere, suggesting that these neurons are not pyramidal. This reinforces the notion that non-specific effects, if present, likely stem from other types of inhibitory neurons. Second, the targeted neuronal populations are, in general, genetically distinct, with the exception of SOM-cre and NOS-cre mice. Third, all the models we tested show slightly different CBF response features. Cross-talk between models would likely show more similar responses between models.

An important consideration in our experiments is that in some mice, YFP expression was biased to the upper layers (see Figure 3). It is possible that some of our results preferentially report regulation properties from cell populations that preferentially exist in upper layers. However, we consistently observed expression spanning Layers III and V, with most variability in Layer VI expression. Inhibitory neurons that preferentially exists in this layer tend to be PV+ or NOS+. In addition, considering that photo-stimulus delivery at the surface of the cortex has difficulty

reaching deeper layers, it is possible that our experiments did not completely capture the role of these cells. Nonetheless, previous experiments from our laboratory suggest that the photo-stimulus parameters chosen influence Layer V/VI neuron activity [9, 25].

Another potential source of variation is that mice were allowed to move and run in our treadmill throughout the experiments. It is possible that the photo-stimulation of the different inhibitory neuron populations elicit different types of activity with different behavioral effects, which might result in unwanted blood flow contributions during recording. In our experience, mice demonstrated little running behavior during experimentation. They were accustomed to the testing apparatus before experiments were conducted, reducing their stress in this environment. Another potential consideration is that motor activity like running is known to increase VIP neuron activation through cholinergic input from the basal forebrain [30], which would impact our VIP-cre mouse results. If the mice were running a considerable amount during stimulation, we would expect to see correspondingly high CBF baseline changes during persistent running periods. Inspection of individual trials from all mice show sparse periods of sustained blood flow that averaged out when averaging multiple experimental trials. This suggests that mice are not running often and that our data is not influenced by changes in blood flow unrelated to the photo-stimulation period.

It is not surprising that NOS and SOM expressing inhibitory neurons are able to regulate or influence local CBF. Nitric oxide is freely diffusible and a potent vasodilator [14, 31]. NOS expressing inhibitory neurons also generally express SOM [14, 23], such that vascular regulation is likely mediated by the activity-dependent release of NO from these neurons. Somatostatin is a neuropeptide that is expressed by Martinotti cells in layer V and interneurons within layers II/III. They are burst or regular spiking and contain vertical arborizations . This neuronal population is

genetically heterogenous, at least compared to PV and VIP expressing inhibitory neurons, with additional sub-types. SOM-expressing inhibitory neurons includes neurons that express NOS, neuropeptide-Y (NPY), calbindin (CB), calretinin (CR), cholecystokinin (CCK) and substance-P [24]. Previous studies have highlighted the role of activating VIP, SOM and NOS neurons on neurovascular coupling and CBF responses. In vitro studies in brain slices with direct electrical stimulation or neuropeptide application showed VIP and NOS neurons produce increases in local microvascular diameter while NPY and SOM produced vasoconstriction [5]. Similar findings were reported in slice experiments by Perrenoud, et al., where neuronal stimulation via bath application of serotonin produced dilations and constrictions [14]. In that study, application of a NPY-receptor antagonist blocked vasoconstriction, while application of a NOS inhibitor blocked vasodilation, indicating that NPY interneurons mediate vasoconstriction and NOS neurons mediate vasodilation. A recent in vivo study corroborated the activity of NPY inhibitory neurons in the generation of vascular constrictions [8]. While we did not study this particular sub-type, our in vivo results are consistent with these reports since photo-stimulation of SOM neurons can target both NOS- and NPY-expressing inhibitory neurons and yielded increases and decreases in CBF following photo-stimulation as observed in Figure 4. In the SOM-cre mice for the 4 second long stimulus-on duration, the increase in CBF appears to occur during the light stimulus period, which we normally disregard due to light interference with the LDF probe. We acknowledge there is a significant increase in CBF during photo-stimulation, but the stimulus energy does not scale with the CBF increases ($p>0.20$). Experiments using an NPY receptor blocker and NOS antagonists would be useful to determine if these two phases of the CBF response in SOM-cre mice can be isolated. In addition, there are two types of nNOS expressing neurons, type I and type II, where type I are few in number and long-projecting while type II are strong NOS expressing and more

numerous [23]. NOS-cre mice target both populations and, assuming both contribute equally to the blood flow response, type II would play a larger role. Lastly, it is worth noting that a small fraction of PV neurons can be targeted in the SOM-cre mouse model we used, which could partly explain the latent increase observed in photo-stimulation responses at higher frequency in these mice [32] (Supplementary Figure 1F).

VIP is expressed by 10-15% of GABAergic cells in the barrel cortex [27]. The largest concentration (60%) of VIP-expressing interneurons is in layer II/III, although VIP cells can be found in all cortical layers, and are anatomically characterized by vertically spanning arborizations that are bipolar/modified-bipolar and bitufted [26, 27]. VIP neurons are not fast-spiking and are active during various brain states including but not limited to locomotion, non-locomotion, visual stimulation, and even under light anesthesia [27, 33]. Optogenetic stimulation of VIP-cre mice showed small increases in blood flow following stimulation that were smaller compared to the whisker CBF response. Nonetheless, our results show some capacity by VIP neurons to generate vasodilations as reported by Cauli [5]. VIP and PV neurons have reciprocal connections, perhaps indicating that small or negligible CBF responses could be due to inhibition of numerous PV neurons. Another plausible contribution could be due to the robust connections of VIP neurons to SOM expressing cells [34]. SOM neurons are known for their connections to distal dendrites of pyramidal cells [22, 34]. It is possible that the activation of VIP neurons can lead to increased inhibition of SOM cells, decreasing the release of NO, where we would expect to see decreases in CBF or attenuated increases. In addition, stimulation of VIP mice for the longer 4 second duration did not show much of a response in blood flow. This could be due to the quiet-and-burst spiking property of some of these neurons [27]. A longer stimulus might not have had much of an effect compared to the short 1 second duration that did allow a quick increase in CBF, similar to quick

bursts of firing. It is difficult to examine or explore these possibilities with our model given the small changes in CBF observed.

Although large numbers of PV+ cells expressed ChR2-YFP, optogenetic stimulation of these cells did not produce typical changes in CBF. Higher stimulus frequencies (20 and 40 Hz) did produce evident latent increases in CBF (Figure 5A and 5B). This is interesting considering PV interneurons comprise about 40% of all GABAergic cells in the cortex [21]. They generally consist of basket and chandelier-shaped cells and are known for their fast spiking, non-adapting properties [28, 35]. In the somatosensory cortex, they are responsible for high frequency gamma oscillations, which are associated with strong cortical network activity. More importantly, gamma oscillation strength is also known to correlate strongly with blood flow changes, including slower hemodynamic fluctuations [36, 37]. The slow increases in CBF observed with PV neuron stimulation support a tight correlation with slow hemodynamic fluctuations. Our findings are different from a previous study where photo-stimulation of PV+ neurons elicited vasoconstriction of local arterioles in brain slices [28]. This difference might be due to in vitro vs. in vivo experimentation. PV neurons are not known for their vasoactive properties, weakly expressing nitric oxide and having no expression of vasoactive intestinal peptide [22, 23]. Though, the evident latent increase in CBF 14-18 seconds post stimulus onset could perhaps be due to NO release from these neurons. Further studies using a NOS antagonist might allow us to determine if NO is responsible or not. Another explanation for the late increase in CBF might be attributed to a rebound in activity from the pyramidal neurons that were previously inhibited, causing an increased demand in blood flow. In addition, their high-frequency spiking properties would imply high metabolic demands upon high-frequency stimulation which might explain the latent increase in CBF we observe with high-frequency photo-stimulation. Alternatively, considering their

abundance in cortex and their connections to other cells (mainly pyramidal cells), they may indirectly regulate blood flow by inhibiting VIP or nitric oxide (NO) release through cortical circuits. Additional studies are necessary to determine the physiological mechanism underlying the slow increases in CBF produced by PV neuron stimulation.

Our results show similarities and differences compared to experiments performed in our laboratory using VGAT-ChR2 mice [9]. Photo-stimulation of VGAT-ChR2 mice under light ketamine anesthesia produced temporal CBF responses that were similar to those produced by NOS and SOM mice in this study. For more direct comparison, we also performed awake head-fixed experiments in VGAT-ChR2 mice (n=4, Supplementary Figure 3). Interestingly, optogenetic stimulation under awake conditions produced CBF responses that peaked a few seconds earlier (and showed a milder modulation to optogenetic pulse duration) compared to our previous study. We verified these CBF response features by performing experiments in these mice under light-ketamine anesthesia (data not shown). In our previous study we also found that pharmacological blockade of NOS suppressed increases in CBF evoked by inhibitory neuron activity [9]. Since VGAT-ChR2 mice target inhibitory neurons, we hypothesize that of photo-stimulation of most inhibitory neurons would produce, at least to first approximation, a weighted combination of photo-stimulating individual sub-populations. This hypothesis of course ignores the impact of initiating activity in sub-populations of inhibitory neurons on network activity and vascular regulation. It is also important to consider that differences in the experimental condition (light anesthesia vs. awake) might make comparisons difficult. Nonetheless, CBF undershoot responses were observed following CBF increases for stronger photo-stimuli (i.e. 30ms pulse duration at 5Hz or 20Hz frequency), but not as evident as those observed in SOM mice. Interestingly, CBF undershoot responses were also observed after NOS blockade in our ketamine-anesthetized VGAT

experiments. Therefore, our studies support the notion that SOM-NPY neuron activity likely generate decreases in CBF.

5.0 Implications and Future Work

Our findings corroborate the strong influence of NOS (and SOM) expressing inhibitory neurons on cerebral blood flow by producing increases in CBF that are similar or even exceed those produced by sensory stimulation. Our findings suggest that dysfunction in NOS neurons likely attenuates the positive CBF response while dysfunction in SOM neurons can work to attenuate both positive (via dysfunction in NOS sub-types) and negative (via dysfunction in NPY sub-types) CBF responses. Our results also show minor influences from PV and VIP inhibitory neurons, suggesting that dysfunction in these neurons will not have as significant of an influence on CBF responses. However, dysfunction in these neuronal populations is likely to have a profound impact on network activity, which might disrupt changes in CBF in a more complicated manner. The metabolic contribution of these neuronal populations also needs to be investigated since changes in local oxygen consumption can also impact fMRI signals.

Lastly, while photo-stimulation of these neuronal populations is essential to determine whether these cell types can modulate local CBF, this mode of stimulation does not engage neuronal activity in a physiological manner. Physiologically relevant approaches could involve pharmacological intervention or the up- and down-regulation of spiking activity using optogenetic silencers, step-function opsins or chemogenetics. These approaches would more directly uncover the impact of dysfunction in specific cell types on local CBF modulation. Our group is currently testing these approaches.

Appendix A - Supplementary Figures

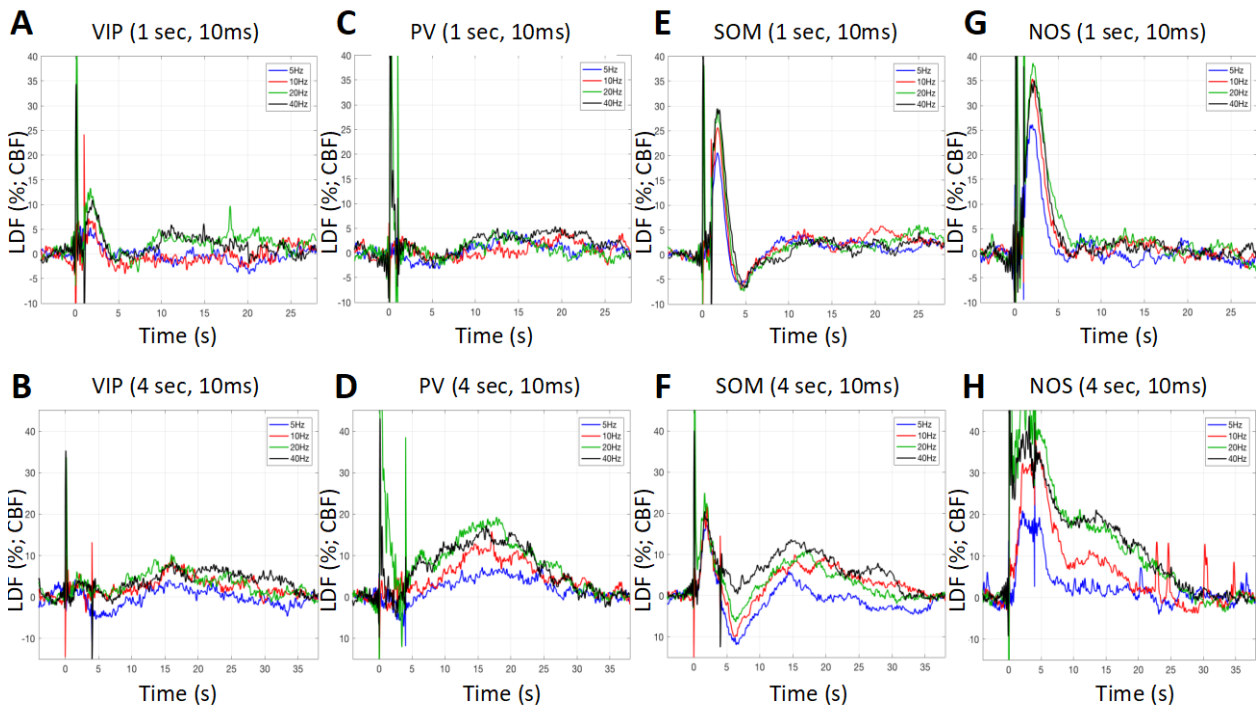

Supplementary Figure 1 - Blood flow response. (A,C,E,G) Average CBF changes in response to photo-stimulation of 10 ms, 1 second stimulus on duration for various pulse frequencies (5 Hz, 10 Hz, 20 Hz, 40 Hz). (B,D,F,H) Average CBF changes in response to photo-stimulation of 10 ms, 4 second stimulus on duration for various pulse frequencies (5 Hz, 10 Hz, 20 Hz, 40 Hz).

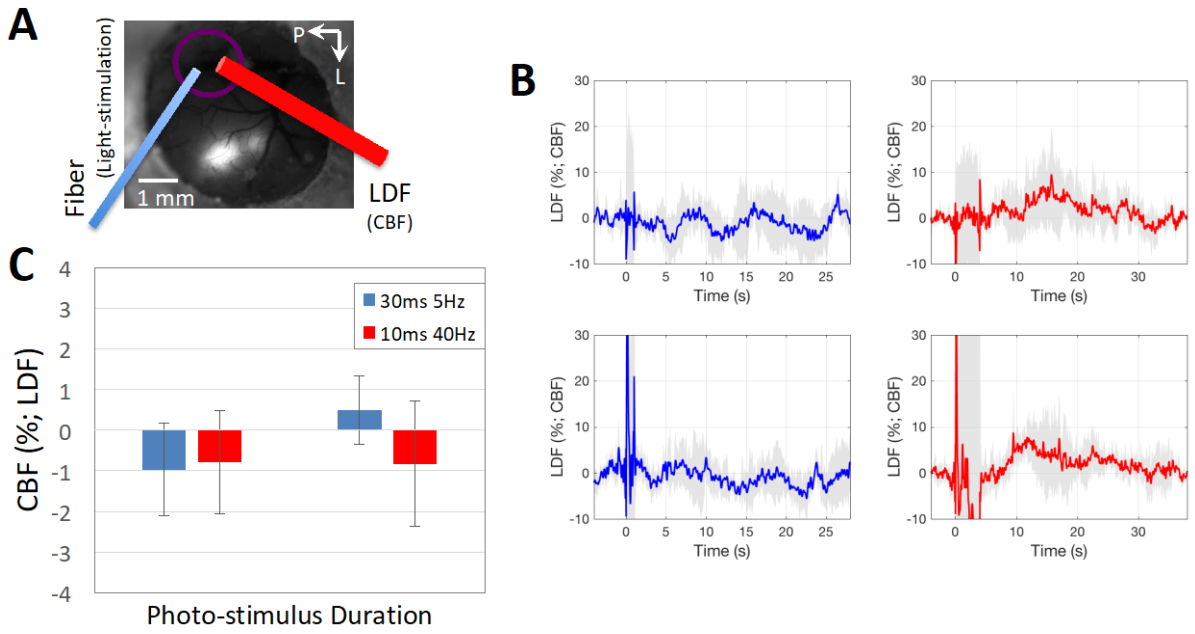

Supplementary Figure 2 - Changes in blood flow measured by LDF in 4 mice (from all strains used) placing the fiber and probe in a non-expressing region. (A) Example image of optic fiber and LDF probe placement in these experiments. (B) Average time series of the CBF changes to the highest energy stimluli used; namely, 30ms 5Hz and 10ms 40Hz pulses delivered for either 1-second or 4-seconds. (C) Bar graph of the average CBF changes following photo-stimulation and the respective standard error. All changes in amplitude were not significantly different from pre-stimulation baseline levels.

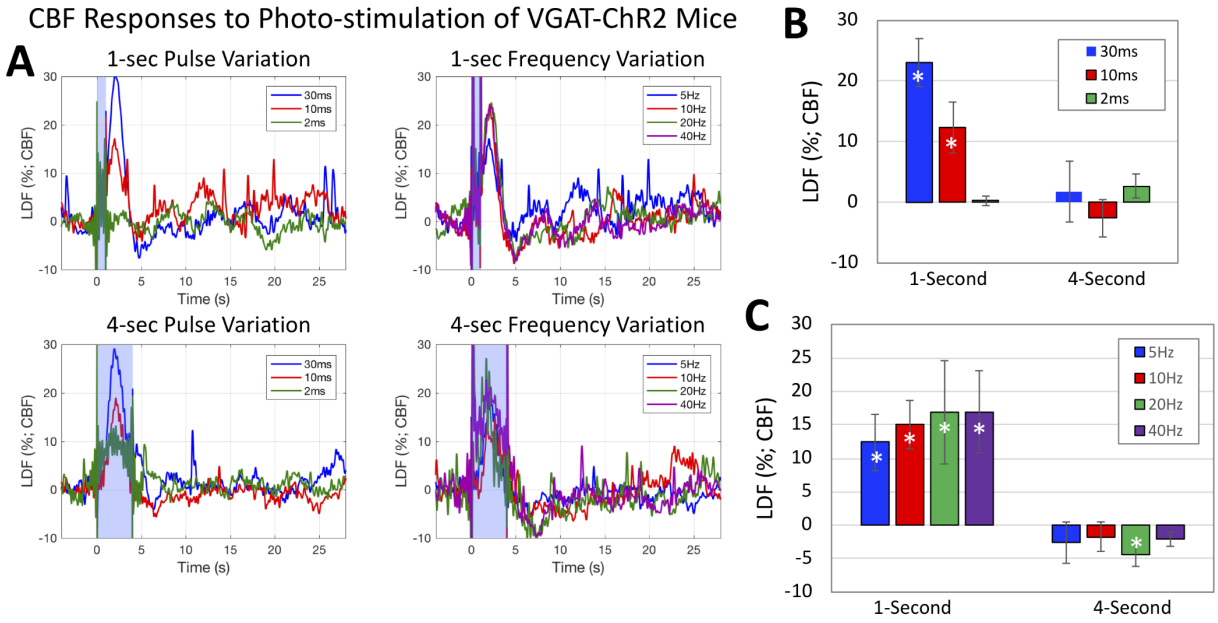

Supplementary Figure 3: (A) Average changes in CBF evoked by photo-stimulation of VGAT-ChR2 mice. CBF responses to 1-sec (top panels), 4-sec (bottom panels), different pulse durations (left panels) and different frequencies (right panels) are presented. The average CBF amplitude immediately following photo-stimulation is compared different pulse widths (B) and different stimulation frequencies (C). Evident increases in CBF were observed after stimulation onset but did not remain significantly elevated after 4-5 seconds for the photo-stimulation parameters used, such that for 4-second photo-stimulation only slight decreases in CBF were observed after stimulus cessation. Significant increases relative to pre-stimulation baseline are indicated by a white star (*, $p<0.05$, panels B and C).

Appendix B Full Figure and Table Captions

Table 1 - Immunostaining summary of the number of neurons expressing ChR2-YFP (YFP-positive or YFP+) in the different inhibitory neuron types of interest (INTI). Total number of cells are reported over all mice examined (number of mice indicated in parenthesis in the first column).

Figure 1 - Experimental setup and experimental paradigm description. (A) Mice were placed under a fluorescence microscope for virus injection in barrel cortex as well as during experiments to identify the expressing region in the somato-sensory cortex for placement of the photo-stimulation optic fiber (473nm light delivery, blue cylinder) and laser Doppler flowmeter (LDF, red probe) for CBF measurements. LDF and the optic fiber were positioned at a 60 degree angle to facilitate placement under the microscope. (B) Sample image taken under green-yellow light (570nm) of the mouse brain while under the microscope illustrating virus injection as well as optic fiber and LDF probe placements (these took place separately during surgical preparation and experimental data collection, respectively). Whiskers were also stimulated by air puffs at 30 psi. (C) Description of the photo-stimulation and whisker-stimulation paradigm. Stimulation was delivered over D seconds every ISI seconds. Trains of stimulation pulses were delivered with duration (d), interval (I) and amplitude (A), repeated N times to match the stimulation period duration (D).

Figure 2 - Fluorescence microscopy images over the entire cranial window (A-D) as well as high resolution two-photon microscopy images (E-H; maximum intensity projections over 10-30μm) of intra-cortical sections from the respective mouse models showing ChR2-YFP expression. In

some mice a red intravascular dye was used to visualize the vasculature (Texas Red Dextran, 50µl 2.5% solution). The inset in panel H shows another image of a nearby neuron. Images of YFP expression were acquired 2-3 weeks after injection. Arrows point towards the whisker region of somato-sensory cortex. The scale bar for the images in each row is located in the left-most image.

Figure 3 - Confocal images of immunostained brain sections from (A) PV, (B) VIP, (C) SOM and (D) NOS mice. For each mouse, larger field-of-view images are shown on the left panels and zoomed images on the right panels (white rectangle on left panels shows zoomed location for images on the right panels). The top panels show staining for the model of interest (red), middle panels show staining for ChR2-YFP (green) and the bottom panels show color merge images. White arrows show location-matched cells between zoomed panels from the same mice.

Figure 4 - Average CBF changes measured by LDF in response to photo-stimulation for 1 second at 5 Hz and various pulse widths (30 ms in blue traces, 10 ms in red traces, 2 ms in green traces), as well as whisker stimulation (black traces) in VIP (A), PV (C), SOM (E) and NOS (G) mice. Similarly, average CBF changes in response to photo-stimulation and whisker for 4 seconds in VIP (B), PV (D), SOM (F) and NOS (H) mice. The photo-stimulus amplitude was fixed to 1mW. The shaded blue rectangle denotes the photo-stimulation period.

Figure 5 - Summary of the changes in CBF evoked by photo-stimulation in the different transgenic mouse models used. Error bars denote standard error. Since typical vascular responses evoked by stimulation peak several seconds after stimulation onset, we measured CBF changes 2-4 seconds after onset for 1-second stimulation (panels A, B, E and F) and 4-7 seconds after onset for 4-second

stimulation (panels C, D, G and H). Significant differences from baseline are denoted by (white *, $p<0.05$). Linear regression analyses were performed to determine whether significant relationships were observed with respect to the photo-stimulus pulse duration (panels E and G) and frequency (panels F and H). Significant relationships are denoted by a (black *, $p<0.05$).

Bibliography

1. Villringer A, and Dirnagl U. Coupling of brain activity and cerebral blood flow: basis of functional neuroimaging. *Cerebrovascular and Brain Metabolism Reviews* 1995; 7(3): 240-276.

2. Ances BM. Coupling of Changes in Cerebral Blood Flow with Neural Activity: What Must Initially Dip Must Come Back Up. *Journal of Cerebral Blood Flow and Metabolism* 2004; 24(1): 1-6.

3. Logothetis N, Pauls J, Augath M, et al. Neurophysiological investigation of the basis of the fMRI signal. *Nature* 2001; 412: 150-157.

4. Hamel E. Perivascular nerves and the regulation of cerebrovascular tone. *Journal of Applied Physiology* 2006; 100(3): 1059-1064.

5. Cauli B. Cortical GABA Interneurons in Neurovascular Coupling: Relays for Subcortical Vasoactive Pathways. *Journal of Neuroscience* 2004; 24(41): 8940-8949.

6. Cauli B, Hamel E. Revisiting the role of neurons in neurovascular coupling. *Frontiers in Neuroenergetics* 2010; 2:9.

7. Anenberg E, et al. Optogenetic stimulation of GABA neurons can decrease local neuronal activity while increasing cortical blood flow. *Journal of Cerebral Blood Flow and Metabolism* 2015; 35(10): 1579-1586.

8. Uhlirova H, Kilic K, Tian P, et al. Cell type specificity of neurovascular coupling in cerebral cortex. *eLife* 2016.

9. Vazquez AL, Fukuda M, and Kim SG. Inhibitory Neuron Activity Contributions to Hemodynamic Responses and Metabolic Load Examined Using an Inhibitory Optogenetic Mouse Model. *Cerebral Cortex* 2018; 28(11): 4105-4119.

10. Sloviter RS. Decreased hippocampal inhibition and a selective loss of interneurons in experimental epilepsy. *Science* 1987; 235(4784): 73-76.

11. Lewis DA, Hashimoto T, Volk DW. Cortical inhibitory neurons and schizophrenia. *Nature Reviews Neuroscience* 2005; 6(4): 312-324.

12. Girouard H, Iadecola C. Neurovascular coupling in the normal brain and in hypertension, stroke, and Alzheimer disease. *Journal of Applied Physiology* 2006; 100(1): 328-335.

13. Iadecola C. Neurovascular regulation in the normal brain and in Alzheimer's disease. *Nature Reviews Neuroscience* 2004; 5(5): 347-360.

14. Perrenoud Q, Rossier J, Ferezou I, et al. Activation of cortical 5-HT(3) receptor-expressing interneurons induces NO mediated vasodilatations and NPY mediated vasoconstrictions. *Frontiers in Neural Circuits* 2012; 6: 50.

15. Cai C, Fordsmann JC, Jensen SH, et al. Stimulation-induced increases in cerebral blood flow and local capillary vasoconstriction depend on conducted vascular responses. *Proc Natl Acad Sci U S A* 2018; 115(25): E5796-E5804.

16. Rugunta RL, Chaigneau E, Osmanski BF, et al. Vascular Compartmentalization of Functional Hyperemia from the Synapse to the Pia. *Neuron* 2018; 99(2): 362-375.

17. Kleinfeld D, Blinder P, Drew PJ, et al. A guide to delineate the logic of neurovascular signaling in the brain. *Frontiers in Neuroenergetics* 2011; 3: 1.

18. Drew PJ, Shih AY, Kleinfeld D. Fluctuating and sensory-induced vasodynamics in rodent cortex extend arteriole capacity. *Proc Natl Acad Sci U S A* 2011; 108(20): 8473-8478.

19. Lecrux C, Toussay X, Kocharyan A, et al. Pyramidal Neurons Are "Neurogenic Hubs" in the Neurovascular Coupling Response to Whisker Stimulation. *Journal of Neuroscience* 2011; 31(27): 9836-9847.

20. Lecrux C and Hamel E. Neuronal networks and mediators of cortical neurovascular coupling responses in normal and altered brain states, *Philosophical Transactions of the Royal Society B: Biological Sciences* 2016; 371(1705).

21. Rudy B, Fishell G, Lee S, et al. Three groups of interneurons account for nearly 100% of neocortical GABAergic neurons. *Developmental Neurobiology* 2011; 71(1) 45-61.

22. Taniguchi H. Genetic dissection of GABAergic neural circuits in mouse neocortex. *Frontiers in Cellular Neuroscience* 2014; 8: 8.

23. Perrenoud Q, Geoffroy H, Gautier B, et al. Characterization of Type I and Type II nNOS-Expressing Interneurons in the Barrel Cortex of Mouse. *Frontiers in Neural Circuits* 2012; 6: 36.

24. Yavorska I and Wehr M. Somatostatin-Expressing Inhibitory Interneurons in Cortical Circuits. *Frontiers in Neural Circuits* 2016; 10: 76.

25. Vazquez AL, Fukuda M, Crowley JC, et al. Neural and hemodynamic responses elicited by forelimb- and photo-stimulation in channelrhodopsin-2 mice: Insights into the hemodynamic point spread function. *Cerebral Cortex* 2014; 24(11): 2908-2919.

26. Connor JR and Peters A. Vasoactive intestinal polypeptide-immunoreactive neurons in rat visual cortex. *Neuroscience* 1984; 12(4): 1027-1044.

27. Prönneke A, Scheuer B, Wagener RJ, et al. Characterizing VIP neurons in the barrel cortex of VIPcre/tdTomato mice reveals layer-specific differences. *Cerebral Cortex* 2015; 25(12): 4854-4868.

28. Urban A, Rancillac A, Martinez L, et al. Deciphering the neuronal circuitry controlling local blood flow in the cerebral cortex with optogenetics in PV:: Cre transgenic mice. *Frontiers in Pharmacology* 2012; 3: 105.

29. Taniguchi H, He M, Wu P, et al. A Resource of Cre Driver Lines for Genetic Targeting of GABAergic Neurons in Cerebral Cortex. *Neuron* 2011; 71(6): 995-1013.

30. Fu Y, Tucciarone JM, Espinosa JS, et al. A cortical circuit for gain control by behavioral state. *Cell* 2014; 156(6): 1139-1152.

31. Iadecola C and Zhang F. Permissive and obligatory roles of NO in cerebrovascular responses to hypercapnia and acetylcholine. *The American Journal of Physiology* 1996; 271(4 Pt. 2): R990-1001.

32. Hu H, Cavendish JZ, Agmon A. Not all that glitters is gold: off-target recombination in the somatostatin-IRES-Cre mouse line labels a subset of fast-spiking interneurons. *Frontiers in Neural Circuits* 2013; 7: 195.

33. Lee S, Kriglikov I, Huang ZJ, et al. A disinhibitory circuit mediates motor integration in the somatosensory cortex. *Nature Neuroscience* 2013; 16(11): 1662-1670.

34. Perrenoud Q, Rossier J, Geoffroy H, et al. Diversity of gabaergic interneurons in layer VIa and VIb of mouse barrel cortex. *Cerebral Cortex* 2013; 23(2): 423-441.

35. Kawaguchi Y and Kubota Y. GABAergic cell subtypes and their synaptic connections in rat frontal cortex. *Cerebral Cortex* 1997; 7(6): 476-486.

36. Mateo C, Knutsen PM, Tsai PS, et al. Entrainment of Arteriole Vasomotor Fluctuations by Neural Activity Is a Basis of Blood-Oxygenation-Level-Dependent 'Resting-State' Connectivity. *Neuron* 2017; 96(4): 936-948.

37. Cardin JA, Carlen M, Konstantinos M, et al. Driving fast-spiking cells induces gamma rhythm and controls sensory responses. *Nature* 2009; 459(7247): 663-667.